Multiplexing Wireless Power Transfer System for EV Charging Stations

Authors
Zhang, Shibo; Dong, Jianning; Bauer, Pavol

DOI
10.1109/WPTCE62521.2025.11062311

Publication date
2025

Document Version
Final published version

Published in
2025 IEEE Wireless Power Technology Conference and Expo, WPTCE 2025 - Proceedings

Citation (APA)
Zhang, S., Dong, J., & Bauer, P. (2025). Multiplexing Wireless Power Transfer System for EV Charging Stations. In *2025 IEEE Wireless Power Technology Conference and Expo, WPTCE 2025 - Proceedings* (2025 IEEE Wireless Power Technology Conference and Expo, WPTCE 2025 - Proceedings). IEEE. https://doi.org/10.1109/WPTCE62521.2025.11062311

Multiplexing Wireless Power Transfer System for EV Charging Stations

1st Shibo Zhang
Department of Electrical Engineering, Mathematics and Computer Science
Delft University of Technology
Delft, the Netherlands
S.Zhang-6@tudelft.nl

2nd Jianning Dong
Department of Electrical Engineering, Mathematics and Computer Science
Delft University of Technology
Delft, the Netherlands
J.Dong-4@tudelft.nl

3rd Pavol Bauer
Department of Electrical Engineering, Mathematics and Computer Science
Delft University of Technology
Delft, the Netherlands
P.Bauer@tudelft.nl

2025 IEEE Wireless Power Technology Conference and Expo (WPTCE) | 979-8-3315-1743-4/25/$31.00 ©2025 IEEE | DOI: 10.1109/WPTCE62521.2025.11062311

***Abstract*— In electric vehicle (EV) charging stations, a common approach to charge multiple EVs is to utilize a shared DC bus for all the converters. However, as the scale of the station grows, this method leads to increased complexity and higher expenses due to the growing number of components. This paper proposes a novel AC multiplexed wireless power transfer (WPT) topology, in which charging modules are connected in parallel on the AC side of a single converter via a highly coupled multi-winding transformer. This topology reduces costs and enables multidirectional power flow for V2X (vehicle-to-vehicle and vehicle-to-grid) applications. In this paper, a comprehensive introduction to the AC multiplexed WPT system is presented, followed by an analysis of its multidirectional power flow characteristics. Finally, a three-port prototype was developed to validate theoretical analysis.**

Keywords—electrical vehicles, wireless power transfer.

I. Introduction

The electric vehicle (EV) industry is experiencing rapid growth, driven by advances in technology and increasing environmental awareness [1]. However, most EVs still rely on wired charging methods, which come with several drawbacks. Wired charging often involves cumbersome cable management, risks of wear and tear, and inconvenience. Wireless charging has emerged as a promising research direction, offering several advantages over wired methods [2]. It eliminates the need for physical connectors, enhancing convenience and reducing maintenance costs. Furthermore, wireless charging systems can improve safety by minimizing exposure to live electrical components and can be seamlessly integrated into urban infrastructure, such as roads and parking spaces, enabling efficient charging-on-the-go [3]. These features make wireless charging an ideal candidate for EV applications. However, despite its potential, wireless charging faces significant barriers to widespread adoption, particularly due to its high costs and complexity [4]. These challenges hinder its large-scale implementation for EV charging. To address this issue, the multiplexing design concept, commonly employed in other industries to reduce system costs and enhance resource utilization, presents a promising solution [6]. Applying this concept to the field of wireless EV charging could not only provide a pathway to more cost-effective and scalable systems, bridging the gap between innovation and practical deployment, but also enable the possibility of achieving multidirectional power flow within the system, supporting functionalities such as V2G (Vehicle-to-Grid) and V2V (Vehicle-to-Vehicle).

ECS4DRES is supported by the Chips Joint Undertaking under grant agreement number 101139790 and its members, including the top-up funding by Germany, Italy, Slovakia, Spain and The Netherlands.

The idea of multiplexing has been used in some research of WPT to realize certain functions. In [6], [7], multiple ports share the same magnetic circuit, enabling arbitrary energy transfer between ports. This significantly enhances system flexibility and reconfigurability. However, the complex coupling relationships between ports lack effective and simplified analytical methods. In [8], the topology with multiple input ports sharing the same compensation network is proposed, where the AC stages of all modules are connected in parallel, while the coils are connected in series, each accompanied by a switch. This topology allows simultaneous charging of multiple loads when all switches are on or charging fewer loads at higher power by turning off certain switches. While this structure offers flexibility in power output, the system design remains relatively complex. In [9], the authors introduce the reuse of a single AC relay coil, enabling wireless power transfer (WPT) among multiple sources and loads without complex cross-coupling between unintended ports. However, the additional power stage increases energy loss and raises system costs. The studies have achieved specific functionalities through design reuse, but often at the expense of increased system complexity. As a result, they are not well-suited for large-scale implementation in wireless charging stations.

In this paper, an AC-multiplexing wireless power transfer system is proposed, where all the charging modules are paralleled and connected to the AC stage of the inverter through a highly coupled transformer. The mutual inductance equivalent model of the system is given. DLCC (Double-side LCC) compensation network of the topology and multidirectional power flow control method are analyzed. Experimental results are provided to validate the theoretical analysis, with details presented in the following sections.

II. Overall System

In traditional EV wireless charging stations, the medium-voltage AC power grid supports a shared DC bus after passing through a transformer and AC-DC rectification, to which all the charging modules are connected, as shown in Fig. 1. A wireless charging module for EV usually consists of an inverter, a compensation circuit, and coils. Connecting multiple charging modules to a same DC bus places the modules in parallel on the DC side of their inverters, allowing charging modules to operate independently. However, this independence necessitates customized module designs to accommodate various EV types and power requirements. Meanwhile, the equipment utilization rate in wireless charging stations is relatively low, and the charging modules are not fully utilized. The downsides mentioned above increase the cost and complexity of EV charging stations.

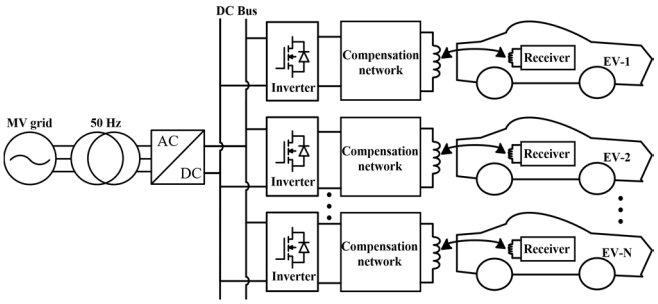

Fig. 1. Traditional arrangements of EV wireless charging stations

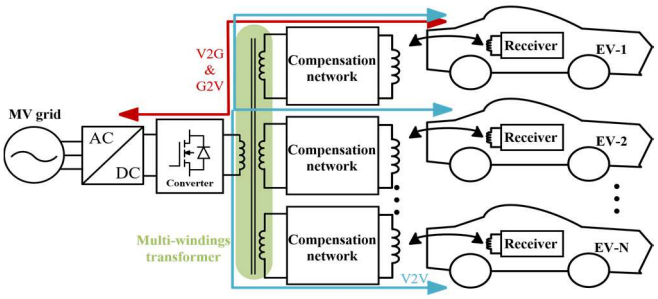

Fig. 2. Proposed AC-multiplexing arrangement for EV wireless charging stations

An AC multiplexed approach for EV wireless charging station is proposed in this paper, as shown in Fig. 2. In the design, all charging modules are paralleled on the ac side of a single converter through a multiport transformer. Compared to traditional designs, this approach eliminates N−1 converters in a station with N wireless charging modules, significantly reducing construction and operational costs. In addition, compared to the low-frequency transformers used in DC-Bus topologies, the proposed topology employs a transformer operating at around 85 kHz (the standard frequency for wireless EV charging). This significantly reduces the transformer's size, making the system more compact. All charging modules coupled to the converter through a multiport transformer enables not only G2V operation but also V2G and V2V functions through appropriate multidirectional power control methods. Given its constant current output characteristics and high-power transmission capability, LCC compensation network is chosen as the compensation network on both sides [10].

III. Modeling of AC-Multiplexing WPT System

A. Mutual Inductance Equivalent Circuit

Fig. 3 shows the mutual inductance equivalent circuit of the proposed system consisting of an input port and N charging modules. U_{in} represents the switching node voltage of the full-bridge converter and can be regarded as a square wave source. A similar analysis applies to the active rectifier on the receiver side of charging module k (k = 1, 2, …, n), where $U_{out\text{-}k}$ denotes the equivalent square wave voltage at its switching node. L_0 is the primary inductance of the transformer while L_k is the secondary inductance. M_{ij} to the mutual inductance between ports i and j in the transformer. In the charging module, $L_{st\text{-}k}$ and $L_{sr\text{-}k}$ are the series inductors on transmission and receiving sides while $C_{st\text{-}k}$ and $C_{sr\text{-}k}$ are the series capacitors on transmission and receiving

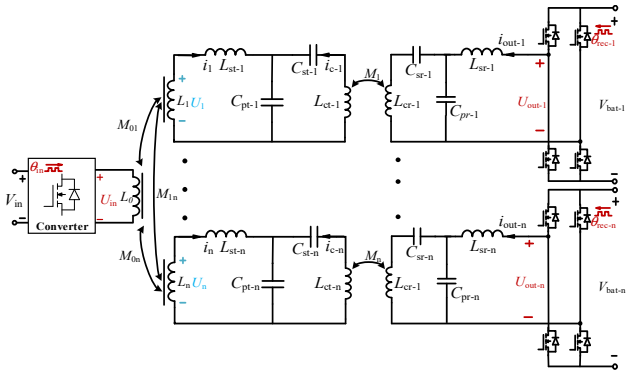

Fig. 3. Mutual Inductance Equivalent Circuit

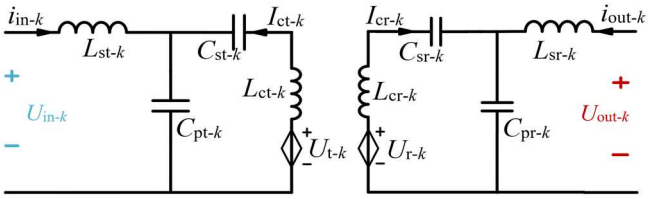

Fig. 4. DLCC compensation network.

sides, respectively. $C_{pt\text{-}k}$ and $C_{pr\text{-}k}$ are the parallel capacitors on transmission and receiving sides. $L_{ct\text{-}k}$ and $L_{cr\text{-}k}$ are the inductances of transmission and receiving coils and M_k donates their mutual inductance.

B. DLCC analysis

To enhance the efficiency and flexibility of wireless power transfer, this study employs a DLCC compensation network. Below, its structure and functionality are analyzed.

Fig. 4 depicts the DLCC structure in the proposed system, where the coupling between coils M_k is modeled as controlled sources in series with their respective coils. They can be written as

$$\begin{cases} \boldsymbol{U}_{t\text{-}k} = -j\omega M_k \cdot \boldsymbol{I}_{cr\text{-}k} \\ \boldsymbol{U}_{r\text{-}k} = -j\omega M_k \cdot \boldsymbol{I}_{ct\text{-}k} \end{cases} \tag{1}$$

Where ω is the angular frequency of the system.

In LCC design, the relationship between inductors and capacitors can be obtained as follows:

$$\begin{cases} \omega^2 = \dfrac{1}{L_{st\text{-}k}C_{pt\text{-}k}} \\ \omega L_{st\text{-}k} = \omega L_{ct\text{-}k} - \dfrac{1}{\omega C_{st\text{-}k}} \end{cases} \tag{2}$$

Based on Kirchhoff's law, the following equation can be achieved in left side LCC network

$$\begin{cases} \boldsymbol{U}_k = \boldsymbol{i}_k \cdot j\omega L_{st\text{-}k} + (-\boldsymbol{i}_{ct\text{-}k}) \cdot \left(\dfrac{1}{j\omega C_{st\text{-}k}} + j\omega L_{ct\text{-}k}\right) + \boldsymbol{U}_{t\text{-}k} \\ \boldsymbol{U}_{t\text{-}k} = \boldsymbol{i}_k \cdot \dfrac{1}{j\omega C_{pt\text{-}k}} + \boldsymbol{i}_{ct\text{-}k} \cdot \left(\dfrac{1}{j\omega C_{st\text{-}k}} + j\omega L_{ct\text{-}k} + \dfrac{1}{j\omega C_{pt\text{-}k}}\right) \end{cases} \tag{3}$$

Apply (2) to (3), $\boldsymbol{i}_k$ and $\boldsymbol{i}_{ct\text{-}k}$ can be obtained as

$$\begin{cases} \boldsymbol{i}_k = j\omega C_{\text{pt-}k} \cdot \boldsymbol{U}_{\text{t-}k} \\ \boldsymbol{i}_{\text{ct-}k} = j\omega C_{\text{pt-}k} \cdot \boldsymbol{U}_k \end{cases} \tag{4}$$

Similarly, on the right side, it can be concluded as

$$\begin{cases} \boldsymbol{i}_{\text{out-}k} = j\omega C_{\text{pr-}k} \cdot \boldsymbol{U}_{\text{r-}k} \\ \boldsymbol{i}_{\text{cr-}k} = j\omega C_{\text{pr-}k} \cdot \boldsymbol{U}_{\text{out-}k} \end{cases} \tag{5}$$

Apply (1) to (4) and (5), relationship between input voltage, output current as well as output voltage, input current can be derived as

$$\begin{cases} \boldsymbol{i}_k = j\omega^3 C_{\text{pt-}k} C_{\text{pr-}k} M_k \cdot \boldsymbol{U}_{\text{out-}k} \\ \boldsymbol{i}_{\text{out-}k} = j\omega^3 C_{\text{pt-}k} C_{\text{pr-}k} M_k \cdot \boldsymbol{U}_k \end{cases} \tag{6}$$

Equation (6) illustrates that despite the structural complexity of the DLCC topology, the relationship between port currents and port voltages remains straightforward: the magnitude of input port current $\boldsymbol{i}_k$ is linearly proportional to the output port voltage $\boldsymbol{U}_{\text{out-}k}$, with a phase lead of 90°. A similar relationship applies to the output current $\boldsymbol{i}_{\text{out-}k}$ and the input voltage $\boldsymbol{U}_{\text{in-}k}$.

C. Power flow control

Phase-shift control is a widely used power regulation method in wireless power transfer, and its principle can be derived from the following equation.

$$\begin{aligned} P_k &= \text{RE}(\boldsymbol{U}_k \boldsymbol{i}_k^*) \\ &= \omega^3 C_{\text{pt-}k} C_{\text{pr-}k} M_k \cdot V_k V_{\text{out-}k} \sin\left(\theta_{\text{out-}k} - \theta_k\right) \end{aligned} \tag{7}$$

Where V_k and $V_{\text{out-}k}$ are the amplitudes of phasor $\boldsymbol{U}_{\text{k}}$ and $\boldsymbol{U}_{\text{out-}k}$. θ_k and $\theta_{\text{out-}k}$ are the angles. Apparently, power can be controlled by adjusting the voltage phase difference between the input and output ports of the DLCC.

On the output side, Given the frequency-selective properties of the LCC network, the fundamental harmonic analysis (FHA) method can be applied. $\boldsymbol{U}_{\text{out-}k}$ can be obtained as

$$\begin{aligned} \boldsymbol{U}_{\text{out-}k} &= V_{\text{out-}k} \angle \theta_{\text{out-}k} \\ &= \frac{2\sqrt{2}}{\pi} V_{\text{bat-}k} \angle \theta_{\text{rec-}k} \end{aligned} \tag{8}$$

where $V_{\text{bat-}k}$ represents the voltage of the battery in EV. $\theta_{\text{rec-}k}$ denotes the driving phase of the upper MOSFET in the full-bridge rectifier, which is aligned with the phase of $U_{\text{out-}k}$.

At the input side, the following expressions can be formulated:

$$\begin{bmatrix} U_{in} \\ U_1 \\ \vdots \\ \vdots \\ U_n \end{bmatrix} = j\omega \begin{pmatrix} L_0 & M_{01} & \cdots & \cdots & M_{0n} \\ M_{10} & L_1 & & & \vdots \\ \vdots & & \ddots & & \vdots \\ \vdots & & & \ddots & \vdots \\ M_{n0} & M_{n1} & \cdots & \cdots & L_n \end{pmatrix} \begin{bmatrix} I_0 \\ -I_1 \\ \vdots \\ \vdots \\ -I_n \end{bmatrix} \tag{9}$$

For any port k, port voltage $\boldsymbol{U}_k$ can be derived from Equation (9) as

$$\begin{aligned} \boldsymbol{U}_k = {} & \frac{M_{k0}}{L_0} \boldsymbol{U}_{in} + j\omega\left(\frac{M_{k0} M_{01}}{L_0} - M_{k1}\right) \boldsymbol{i}_1 + \cdots \\ & + j\omega\left(\frac{M_{k0} M_{0k}}{L_0} - L_k\right) \boldsymbol{i}_k + \cdots + j\omega\left(\frac{M_{k0} M_{0n}}{L_0} - M_{kn}\right) \boldsymbol{i}_n \end{aligned} \tag{10}$$

For mutual inductance, the following formula is applicable

$$M_{ij} = k_{ij} \sqrt{L_i L_j} \tag{11}$$

Where k_{ij} denotes the mutual inductance coefficient between module i and j. Given the strong coupling characteristics between windings in the transformer, it is assumed that the mutual inductance coefficient between any pair of windings is equal: $k_{ij} = k_{\text{m}}$. Equation (10) can be simplified as

$$\begin{aligned} \boldsymbol{U}_k = {} & k_m \sqrt{\frac{L_k}{L_0}} \boldsymbol{U}_{in} + j\omega\left(k_m^2 - k_m\right) \sqrt{L_k L_1} \boldsymbol{i}_1 + \cdots \\ & + j\omega\left(k_m^2 - 1\right) L_k \cdot \boldsymbol{i}_k + \cdots + j\omega\left(k_m^2 - k_m\right) \sqrt{L_k L_n} \boldsymbol{i}_n \end{aligned} \tag{12}$$

Based on equation (7)(8)(12), the final expression is

$$\begin{aligned} P_k = {} & \frac{8 k_m}{\pi^2} \sqrt{\frac{L_k}{L_0}} V_{in} V_{bat} \omega^3 C_{\text{pt-}k} C_{\text{pr-}k} M_k \sin(\theta_{\text{rec-}k} - \theta_{in}) + \\ & \frac{8\omega^7 C_{\text{pt-}k} C_{\text{pr-}k} M_k (k_m - k_m^2) V_{\text{bat-}k} \sqrt{L_k}}{\pi^2} \sum_{p=1, p\neq k}^{n} C_{\text{pt-}p} C_{\text{pr-}p} M_p V_{\text{bat-}p} \sqrt{L_p} \sin(\theta_{\text{rec-}k} - \theta_{\text{rec-}p}) \end{aligned} \tag{13}$$

The power of charging module k comes from two sources: the power grid and other charging modules. Notably, when k_{m} approaches 1 and k_{m}-k_{m}^2 approaches 0, the first term in the equation — representing the power input from the grid — dominates under proper phase settings, significantly exceeding the contribution from other modules. When the phase of the grid-side converter leads to that of the receiver-side converter, the EV delivers power to the grid, operating in V2G mode. Conversely, when the phase lags, the system operates in G2V mode. This also indicates that for a multi-terminal wireless charging station, adopting this topology allows for V2V charging and even vehicle-to-storage (V2Storage) charging by adjusting the phases of converters.

IV. Experimental Result

To validate the proposed topology, experiments were carried out using a three-port WPT prototype, which is depicted in Fig. 5. The system consists of one input and two outputs. A single inverter generates high-frequency AC, which is fed into a multi-winding transformer. Each secondary winding is connected to its own DLCC compensation network, coils, and rectifier. Each port is connected to a bidirectional DC power source, which can operate either as a load or as a source. The power flow for each port is controlled by signals generated from TI Launchpads F28379D boards. Detailed parameters of the prototype can be found in Table. I.

TABLE I.
EXPERIMENTAL PARAMETERS

Symbol	Parameters	Value
f	frequency	85kHz
K_m	Transformer Mutual inductance coefficient	0.99
$L_{ct\text{-}1}$, $L_{cr\text{-}1}$	Output 1 Coil inductances	335.8, 224.7 μH
$L_{ct\text{-}2}$, $L_{cr\text{-}2}$	Output 2 Coil inductances	60.8, 61.2 μH
$L_{st\text{-}1}$, $L_{sr\text{-}1}$	Output 1 Series inductances	103.8, 83.8 μH
$L_{st\text{-}2}$, $L_{sr\text{-}2}$	Output 2 Series inductances	31.3, 34.8 μH
$C_{pt\text{-}1}$, $C_{pr\text{-}1}$	Output 1 Parallel capacitances	33.1, 41.3 nF
$C_{pt\text{-}2}$, $C_{pr\text{-}2}$	Output 2 Parallel capacitances	112.3, 101.1 nF
M_1, M_2	Coils Mutual inductances	95.0, 25.6 μH

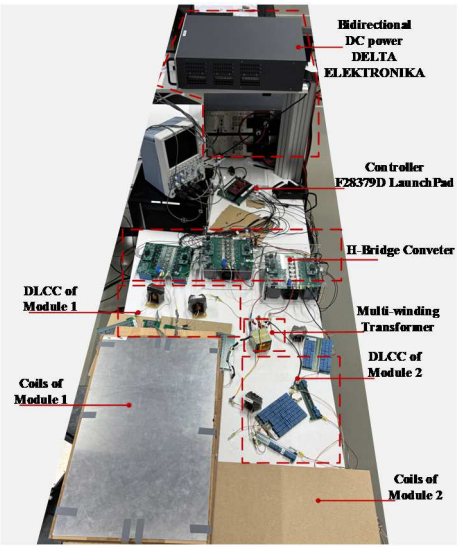

Fig. 5. Experimental prototype

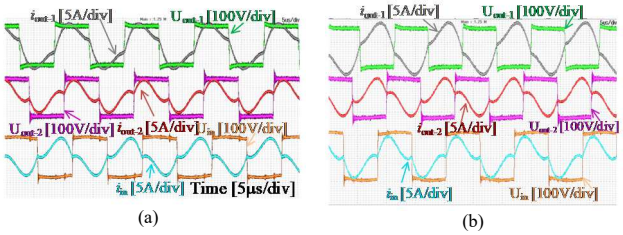

(a) (b)

Fig. 6. Steady-state voltage and current waveforms of Converter Ports under G2V and V2G modes: (a) G2V Mode. (b) V2G Mode.

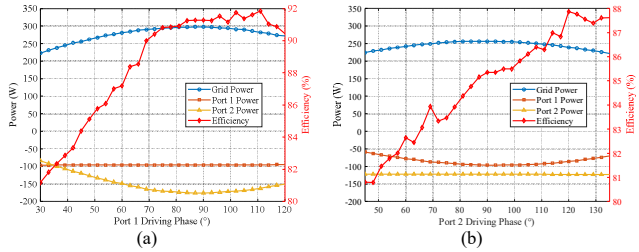

(a) (b)

Fig. 7. Power and efficiency versus driving phase: (a) Port 1; (b) Port 2.

Figure 6 shows the steady-state waveforms under G2V and V2G modes, which were sampled at the following positions in the circuit: U_{in} and i_{in} were Measured at the input side of the full-bridge inverter, before the primary side of the transformer. $U_{out\text{-}1}$, $i_{out\text{-}1}$, $U_{out\text{-}2}$, and $i_{out\text{-}2}$ were Measured at the output of each DLCC compensation network, immediately before entering the rectifier stage. In G2V mode, the driving signals for each port are set as follows: $\theta_{in} = 0°$, $\theta_{out\text{-}1} = 90°$, $\theta_{out\text{-}2} = 45°$. Energy flows from the input side into both outputs, primarily toward output port 1. In V2G mode, the driving signals are set as follows: $\theta_{in} = 90°$, $\theta_{out\text{-}1} = 0°$, $\theta_{out\text{-}2} = 45°$. The waveform confirms this bidirectional flow $i_{out\text{-}1}$ and $i_{out\text{-}2}$ now exhibits reversed current direction compared to G2V mode, indicating that both the outputs are supplying energy back to the input. The system demonstrates the feasibility of flexible bidirectional power control via phase shift modulation.

The experimental conditions for Fig. 7 are as follows. In Fig. 7(a), the phase shift of the inverter at the grid side is fixed at 0°, the driving phase of Port 2 is fixed at 45°, and the driving phase of Port 1 is swept from 30° to 120°. In Fig. 7(b), the phase shift of the inverter at the grid side is also fixed at 0°, the driving phase of Port 1 is fixed at 90°, and the driving phase of Port 2 is swept from 45° to 135°. The voltage at the grid side is set to 100 V, and the voltages at both Port 1 and Port 2 are set to 80 V. The overall system efficiency remains relatively high, ranging from approximately 82% to 92% across the experiments.

These two subfigures mainly serve to validate that although the multiport transformer magnetically couples all ports, when the mutual coupling coefficient approaches 1, the ports become nearly decoupled. This means that by adjusting the phase difference between any port and the grid-side converter, the power of that port can be regulated almost independently. This conclusion was previously derived in Equation (13), and the experimental results shown here provide further confirmation. Specifically, in Figure 7(a), as the phase of Port 1 is varied, the power at Port 2 remains almost constant, and the maximum power of Port 1 occurs near a phase difference of 90°. A similar result can be observed in Figure 7(b), where sweeping the phase of Port 2 has minimal impact on Port 1, and the power of Port 2 reaches its peak around 90°.

V. CONCLUSION

This article proposed a multiplexing wireless power transfer system with the implementation of a multi-windings transformer. Through multiplexing design, the proposed system significantly reduces the number of components compared to traditional wireless charging stations for electric vehicles. This not only lowers the station's cost but also makes the system more compact. Theoretical analysis demonstrates that phase-shift control is well-suited for this system, enabling arbitrary power flow and supporting V2G functionality. The experimental validation using a prototype with one input and two output ports confirms the feasibility of the proposed multiplexed WPT system architecture. Flexible bidirectional power transfer between the input and outputs is achieved using phase shift modulation, and near-independent control of each output port is verified despite the magnetic coupling inherent in the multiport transformer. Additionally, the system maintains relatively high efficiency throughout the experiments, further confirming the practicality of the proposed design.

REFERENCES

[1] G. Zhu, J. Dong, T. B. Soeiro, H. Vahedi and P. Bauer, "Dual-Side Capacitor Tuning and Cooperative Control for Efficiency-Optimized Wide Output Voltages in Wireless EV Charging," in IEEE Transactions on Industrial Electronics.

[2] H. Yin, M. Fu, M. Liu, J. Song and C. Ma, "Autonomous Power Control in a Reconfigurable 6.78-MHz Multiple-Receiver Wireless Charging System," in IEEE Transactions on Industrial Electronics, vol. 65, no. 8, pp. 6177-6187, Aug. 2018.

[3] I. Q. Deng, P. Sun, W. Hu, D. Czarkowski, M. K. Kazimierczuk and H. Zhou, "Modular Parallel Multi-Inverter System for High-Power Inductive Power Transfer," in IEEE Transactions on Power Electronics, vol. 34, no. 10, pp. 9422-9434, Oct. 2019.

[4] A. Mahesh, B. Chokkalingam and L. Mihet-Popa, "Inductive Wireless Power Transfer Charging for Electric Vehicles–A Review," in IEEE Access, vol. 9, pp. 137667-137713, 2021.

[5] M. Tamura, K. Murai and M. Matsumoto, "Design of Conductive Coupler for Underwater Wireless Power and Data Transfer," in IEEE Transactions on Microwave Theory and Techniques, vol. 69, no. 1, pp. 1161-1175, Jan. 2021.

[6] Y. Chen, P. Wang, Y. Elasser and M. Chen, "Multicell Reconfigurable Multi-Input Multi-Output Energy Router Architecture," in IEEE Transactions on Power Electronics, vol. 35, no. 12, pp. 13210-13224, Dec. 2020.

[7] Y. Wang, M. Liu and M. Zhu, "Power Flow Control and ZVS Condition Analysis in Multiport Wireless Energy Router," 2024 IEEE Wireless Power Technology Conference and Expo (WPTCE), Kyoto, Japan, 2024, pp. 754-758.

[8] Y. Zhang, D. Lan, X. Mao and Y. Zhuang, "Modular Wireless Power Transfer Systems for Charging Stations Based on a Common AC Bus With LCC Compensation," in IEEE Journal of Emerging and Selected Topics in Power Electronics, vol. 12, no. 3, pp. 3268-3276, June 2024.

[9] M. Zhou, F. Liu, K. Lu and X. Chen, "Modular Stacked Multiport Wireless Energy Interconnection System With Virtual AC Bus and Its Power Flow Control Strategy," in IEEE Transactions on Power Electronics, vol. 37, no. 12, pp. 15774-15784, Dec. 2022.

[10] W. Li, H. Zhao, J. Deng, S. Li and C. C. Mi, "Comparison Study on SS and Double-Sided LCC Compensation Topologies for EV/PHEV Wireless Chargers," in IEEE Transactions on Vehicular Technology, vol. 65, no. 6, pp. 4429-4439, June 2016.